Inorganic Chemistry

Article

pubs.acs.org/IC

Potassium–Sulfur Batteries: A New Member of Room-Temperature Rechargeable Metal–Sulfur Batteries

Qing Zhao, Yuxiang Hu, Kai Zhang, and Jun Chen*

Key Laboratory of Advanced Energy Materials Chemistry (Ministry of Education), Collaborative Innovation Center of Chemical Science and Engineering (Tianjin), College of Chemistry, Nankai University, Tianjin 300071, People's Republic of China

Supporting Information

ABSTRACT: We report room-temperature rechargeable potassium–sulfur (K-S) batteries using ordered mesoporous carbon (CMK-3)/sulfur and polyanilime (PANI) coated CMK-3/sulfur composites as the cathode and metallic potassium as the anode. The electrochemical reaction mechanism was investigated by electrochemical tests, TEM, XRD, and Raman spectra. It was found that K-S batteries delivered two reduction peaks located at about 2.1 and 1.8 V and one oxidation peak at about 2.2 V, respectively. Meanwhile, K_2S_3 was the major discharge product that could be charged to reversibly form S and K ion. Through optimization of sulfur content, the CMK-3/sulfur composite with 40.8 wt % S displayed an initial discharge capacity of 512.7 mAh g^{-1} and a capacity of 202.3 mAh g^{-1} after 50 cycles at a current density of 50 mA g^{-1}. A coating of conductive polyanilime (PANI) on the CMK-3/sulfur composite is effective in enhancing the cycling performance. In comparison, PANI@CMK-3/sulfur composite showed a capacity of 329.3 mAh g^{-1} after 50 cycles at 50 mA g^{-1}. The results shed light on the basic study of rechargeable K-S batteries.

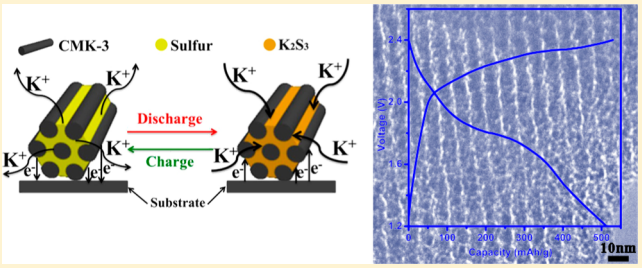

INTRODUCTION

Room-temperature metal (Li,[1−9] Na,[10−16] Mg,[17−19] Ca[20])–sulfur batteries have attracted extensive interest due to their advantages of high theoretical capacity, high elemental abundance, low cost, and environmental friendliness. As a member of the light metals, K has been paid little attention in application of batteries because of its overactive chemical properties. However, several natural superiorities of K anodes cannot be ignored, such as low standard electric potential ($E°(Li^+/Li) = -3.04$ V, $E°(K^+/K) = -2.93$ V, $E°(Ca^{2+}/Ca) = -2.87$ V, $E°(Na^+/Na) = -2.71$ V, $E°(Mg^{2+}/Mg) = -2.27$ V, all vs standard hydrogen redox potential), abundant presence in nature, and low price. Moreover, recent studies have shown that metal K exhibits amazing properties in metal–oxygen batteries with the lowest overpotential (less than 50 mV).[21,22] In addition, an aqueous K ion battery with nickel hexacyanoferrate also shows superior properties to insert and extract potassium ions.[23] As metal–oxygen and metal–sulfur batteries share numerous similarities,[24,25] it is interesting and necessary to do the research on room-temperature K-S batteries.

Metal–sulfur batteries usually face a few common troubles, such as the insulating nature of sulfur, dissolution of polysulfides, and the volume expansion from sulfur to the discharge product of metal sulfides.[26−28] Two main strategies have been applied to solve these problems. One is encapsulating sulfur into various carbon materials,[29−35] and the other is wrapping sulfur with conductive polymers.[36] In particular, CMK-3, as a well-known highly ordered mesoporous carbon material,[37,38] has been successfully used in Li-S batteries.[39] CMK-3 not only limits the volume expansion from S to Li_2S but also improves the electronic conductivity. Meanwhile, polyaniline (PANI) is also a star conductive polymer which could reduce the solvation of polysulfides and improve the cycling performance.[40−42] Thus, it is natural to ask about the combination of CMK-3 and PANI with sulfur as the cathode material of rechargeable K-S batteries.

In this work, we reported on the synthesis of a series of CMK-3/sulfur composites with different contents of S through a frequently used method with a melt-diffusion process. The optimalizing composite with the proper content of S was further coated by PANI through an in situ polymerization at a freezing temperature. The electrochemical performance of metal K-S batteries with the as-prepared composite as cathode materials was tested at room temperature. According to the analysis of TEM, XRD, and Raman spectra, the reaction mechanism during discharge–charge was also confirmed. It is confirmed that K_2S_3 was formed during the discharge process and decomposed back to K ion and sulfur after the charge (Figure 1). Galvanostatic tests showed that the composite with 40.8 wt % S delivered an initial discharge capacity of 512.7 mAh g^{-1} at a charge/discharge current density of 50 mA g^{-1}, which is about 91.9% of the theoretical capacity (558 mAh g^{-1}) on the basis of the sulfur content. The discharge capacity after 50 cycles at 50 mA g^{-1} was 202.3 mAh g^{-1}. After polyaniline coating, the cycling performance was further enhanced and a

Received: April 21, 2014
Published: August 13, 2014

   dx.doi.org/10.1021/ic500919e | Inorg. Chem. 2014, 53, 9000–9005

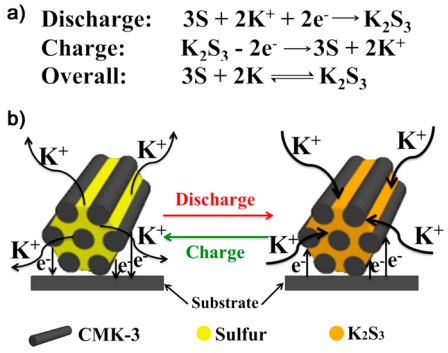

Figure 1. (a) Discharge, charge, and overall reaction. (b) Schematic diagram of electrode reactions of rechargeable K-S batteries.

capacity of 329.3 mAh g^{-1} was maintained after 50 cycles at the same current density.

EXPERIMENTAL SECTION

Synthesis of CMK-3/Sulfur Composites. Different weight ratios of CMK-3/sulfur composites were fabricated through a melt-diffusion method. In a typical experiment for the synthesis of CMK-3/sulfur composite with 40.8 wt % S, 0.6 g of CMK-3 (JCNANO) and 0.4 g of sublimed sulfur were weighed and ground homogeneously in a mortar. The mixture was put into a sealed vessel, under the protection of argon. Then, the composites were heated to 155−160 °C at a heating rate of 5 °C/min. The temperature was maintained for 12 h. The CMK-3/sulfur composite was obtained after natural cooling. The composites with 20.8 wt % S, 59.2 wt % S, and 78.0 wt % S were respectively obtained by weighing 0.4 g of CMK-3 and 0.1 g of S, 0.4 g of CMK-3 and 0.6 g of S, and 0.2 g of CMK-3 and 0.8 g of S before blending.

Synthesis of PANI@CMK-3/Sulfur Composite. The CMK-3/sulfur composite with about 50 wt % S was applied to coat PANI to give a similar 40 wt % S content composite as a comparison. In brief, 0.2 g of CMK-3/sulfur composite was put into a round-bottomed flask which contained 15 mL of distilled water and 2 mL of acetone. Then, 0.06 g of aniline and 10 mL of dilute hydrochloric acid solution (2 mol/L) were added into the flask and the mixture was stirred vigorously. An aqueous solution of $(NH_4)_2S_2O_8$ (0.12 g) as an oxidant was added dropwise. After the mixture was stirred for 7 h, the precipitate was filtered and washed with distilled water and acetone. The PANI@CMK-3/sulfur composite was obtained after drying in a vacuum oven.

Materials Characterization. Instrumental analyses of structure and morphologies were applied to characterize the as-prepared materials. Powder X-ray diffraction was carried out in the 2θ range of 10−80° (Rigaku MiniFlex600, Cu Kα radiation) and 0.6−2.5° (Bruker D8 FOCUS, Cu Kα radiation). The content of S was calculated by thermogravimetric analysis (TGA) using a TG-DSC analyzer (NETZSCH, STA 449 F3)[43] with a heating rate of 5 °C/min from room temperature to 800 °C in an air atmosphere. The Brunauer−Emmett−Teller (BET) specific surface area was analyzed through calculation of the N_2 adsorption−desorption isotherm at 77 K on a BELSORP-mini instrument. The morphology and microstructure of CMK-3/sulfur composites were observed by field-emission scanning electron microscopy (SEM, JEOL JSM7500F) and transmission electron microscopy (TEM, Philips Tecnai FEI). The FTIR spectra were recorded using KBr pellets on an AVATAR 360 spectrometer (Nicolet Instrument Corp., USA) in the wavelength range 400−4000 cm^{-1}.

Cell Assembly and Electrochemical Test. The CR2032 coin type cells were assembled as detailed in our previous reports.[44,45] The cathodes were fabricated by blending synthetic composites, super P, and polytetrafluoroethylene (PTFE) in ethanol with a weight ratio of 8:1:1. The obtained slurry was pasted onto an aluminum foil and dried at 80 °C for 12 h in a vacuum oven. The anode was potassium thin foil that was cut into round pieces. The electrolyte was 1.0 M $KClO_4$ in tetraethylene glycol dimethyl ether (TEGDME). The coin cells were assembled in an argon-filled glovebox (Mikrouna Universal 2440/750) with oxygen level and moisture content below 1 ppm. The electrochemical tests were carried out at room temperature. Cyclic voltammograms (CVs) were recorded with a PARSTAT electrochemical workstation (Princeton Applied Research & AMETEK Co.).[46] A LAND (Wuhan, People's Republic of China) battery testing instrument was applied for galvanostatic charge−discharge tests.[47] Electrochemical impedance spectroscopy (EIS) was measured with an ac voltage of 10 mV amplitude in the frequency range from 100 kHz to 100 mHz.

Analysis of the Discharge and Charge Products. The loss of sulfur was calculated through weighing the cathode before cycling and after 50 cycles (a detailed method is provided in the calculation of sulfur content in the cathode in the Supporting Information). To further analyze the process of the K-S battery system, the cathode with 78.0 wt % S was chosen to observe the major product for the reason that sulfur signal could be detected in this proportion. At a lower content such as 20.9 or 40.8 wt %, sulfur has been completely impregnated into the pores of CMK-3 and no sulfur peaks could be detected. Indeed, the major signal of the discharge cathode is covered with the carbon. The discharge and charge product was characterized by an ex situ means. The discharge cathode was protected by parafilm, which was able to prevent the material from being destroyed by water in a relatively small amount of time.[48] By use of a confocal Raman microscope (DXR, Thermo Fisher Scientific) with excitation at 532 nm from an argon ion laser, Raman spectra were collected. The XRD spectra and TEM images were obtained as detailed above.

RESULTS AND DISCUSSION

The as-synthesized CMK-3/sulfur composites were characterized by various instrumental analyses. The weight ratio of sulfur was calculated according to the result of thermogravimetric analysis (Figure S1, Supporting Information). The contents of S in CMK-3/sulfur composites were analyzed as 20.9%, 40.8%, 59.2%, and 78.0% (by weight). Low-angle XRD patterns (Figure 2a) in the 2θ range of 0.6−2.5° suggest proper S content. The sharp peak located at 1.3° proves the highly ordered mesoporous structure of CMK-3. When sulfur was flowed into the pores of CMK-3, the sharp peak at 1.3° disappeared step by step. In this case, CMK-3/sulfur composite with a proper S content could be optimized. SEM images

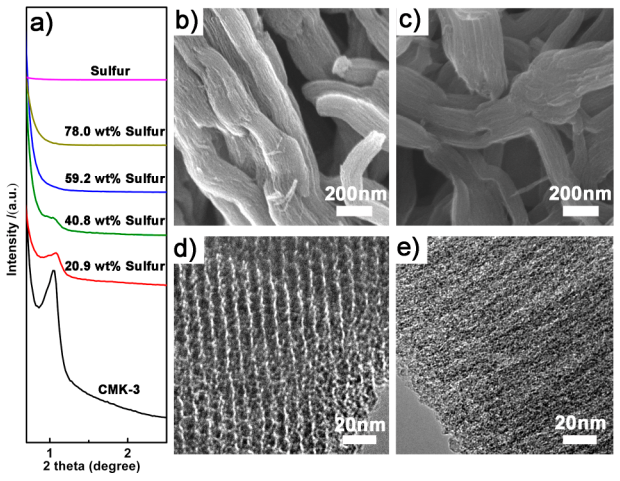

Figure 2. (a) Low-angle XRD patterns of CMK-3, CMK-3/sulfur composites with selected S content. (b, c) SEM and (d, e) HRTEM images of (b, d) CMK-3 and (c, e) CMK-3/sulfur composite with 40.8 wt % S.

dx.doi.org/10.1021/ic500919e | Inorg. Chem. 2014, 53, 9000−9005

(Figure 2b,c) reveal that the surfaces of CMK-3 and CMK-3/sulfur (with 40.8 wt % S) are similar. However, an analysis of TEM images (Figure 2d,e) shows that the pores of CMK-3 are filled by sulfur. From the corresponding elemental mappings of TEM, we can visually see the homogeneous distribution of sulfur (Figure S2, Supporting Information). SEM images of CMK-3/sulfur composites with the other S contents (Figure S3, Supporting Information) prove that S is gradually overflowed on the surface of CMK-3 with increasing sulfur content. The XRD patterns in the 2θ range of 10−80° (Figure S4, Supporting Information) show that no sharp diffraction peaks of S have been observed when the S content is lower than 59.2 wt %. When the content of S is increased, the peaks of sulfur gradually arise as a portion of S covering the surface of CMK-3. It is noted that the specific surface area and pore volume also reduced one by one as S was impregnated in the pores of CMK-3 (Table S1, Supporting Information). On consideration of enough space for insertion of K ion, a CMK-3/sulfur composite with 40.8 wt % S is proposed to be a proper sample.

Electrochemical measurements on CMK-3/sulfur composites were carried out by assembling a CR2032 coin cell.[49] The voltage region between 1.2 and 2.4 V was selected for electrochemical tests in order to achieve better cycling performance (higher voltage region, Figure S5, Supporting Information). Figure 3a shows the structure of a K-S battery.

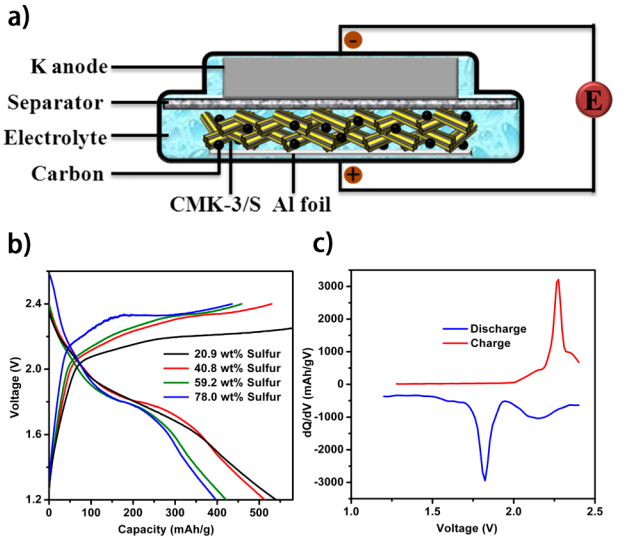

Figure 3. (a) Schematic illustration of a K-S battery. (b) Initial discharge and charge curves of K-S batteries using CMK-3/sulfur composites with different contents of S as the cathode at a current density of 50 mA g^{-1}. (c) Corresponding differential capacity plots of 40.8 wt % S cathode.

Figure 3b displays the initial discharge and charge curves of K-S batteries with different contents of S at a current density of 50 mA g^{-1}. The discharge capacity consecutively decreased from 540.5 to 396.8 mAh g^{-1} with increasing S content from 20.9 to 78.0 wt %. It can be seen that, in the discharge curves, a gentle slope followed by a discharge platform (at about 1.8 V) was observed, indicating two steps of the discharge process. This means that sulfur was first reduced to high-chain polysulfides and further reduced to low-chain polysulfides. In the charge process, a long single platform was detected, which showed that the low-chain polysulfides were oxidized in one step. The discharge platform is slightly higher than that for Na-S batteries, whose discharge curves consist of a sloping region and a platform at 1.66 V by using similar ether (TEGDME) based electrolyte.[16] This is caused by different standard electric potentials of K and Na ($E°(K^+/K) = -2.93$ V, $E°(Na^+/Na) = -2.71$ V). Figure 3c gives the corresponding differential capacity plots of 40.8 wt % S cathode. From Figure 3c, it is seen that K-S batteries have two steps in the discharge process and one step in the charge process. Taking both S content and discharge capacity into account, CMK-3/sulfur composite with 40.8 wt % S was specially analyzed in the next electrochemical test.

Figure 4a shows the cyclic voltammograms carried out at a scan rate of 0.1 mV s^{-1} between 1.2 and 2.4 V. Two reduction

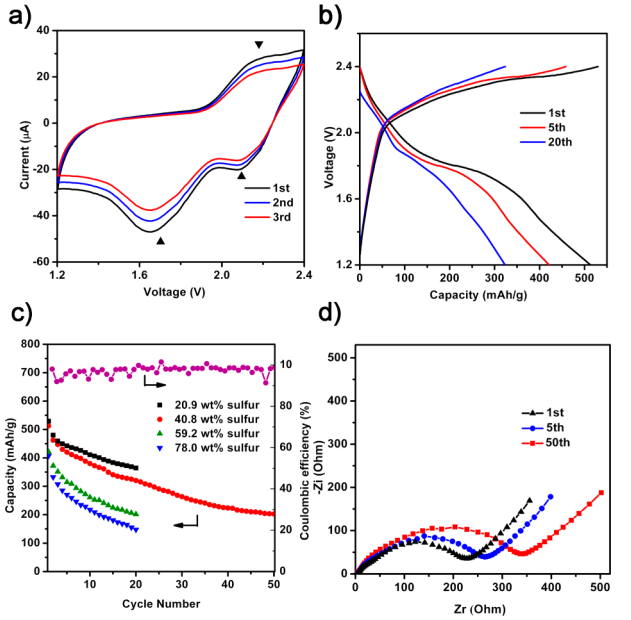

Figure 4. Electrochemical tests of CMK-3/sulfur composite with 40.8 wt % S: (a) cyclic voltammograms at a scan rate of 0.1 mV s^{-1} between 1.2 and 2.4 V; (b) galvanostatic discharge−charge profiles at 50 mA g^{-1}; (c) cycling performance with different contents of S at 50 mA g^{-1} and Coulombic efficiency of selected 40.8 wt % S cathode; (d) electrochemical impedance spectra collected at 1.8 V at different cycles.

peaks and one oxidation peak are detected, which inosculate well with the corresponding differential capacity plots. On the second cycle, the intensities of both oxidation and reduction peaks become weaker; this phenomenon was caused by the dissolution of potassium polysulfides (K_2S_x) to cause a loss in quality of the cathode. Figure 4b shows selected discharge and charge profiles of K-S batteries using CMK-3/sulfur composite with 40.8 wt % S at 50 mA g^{-1}. The initial discharge and charge capacities are 512.7 and 522.5 mAh g^{-1}, respectively. The capacity is 421.6 mAh g^{-1} in the 5th cycle and 321.4 mAh g^{-1} in the 20th cycle. Figure 4c displays the cycling performance of CMK-3/sulfur composites with different contents of S at 50 mA g^{-1}. The capacity decays quickly when the S content in CMK-3/sulfur composites is higher than 40.8 wt %. After 50 cycles, the discharge capacity of CMK-3/sulfur composite with 40.8 wt % S remains 202.3 mAh g^{-1}, which is approximately 39.4% capacity retention. The Coulombic efficiencies are all above 90%. Figure 4d shows the electrochemical impedance spectra of CMK-3/sulfur composite with 40.8 wt % S. The

dx.doi.org/10.1021/ic500919e | Inorg. Chem. 2014, 53, 9000−9005

spectra were collected at a voltage of 1.8 V, where the discharge platform is located. It could be seen that the resistance increases with cycling, which could be derived from the insolubility of the low-chain polysulfides deposited on the surface of the electrode.

The synthetic CMK-3/sulfur composite was further coated by PANI to improve the electrochemical properties. A TEM image (Figure 5a) visually proves that the skeleton of CMK-3 is

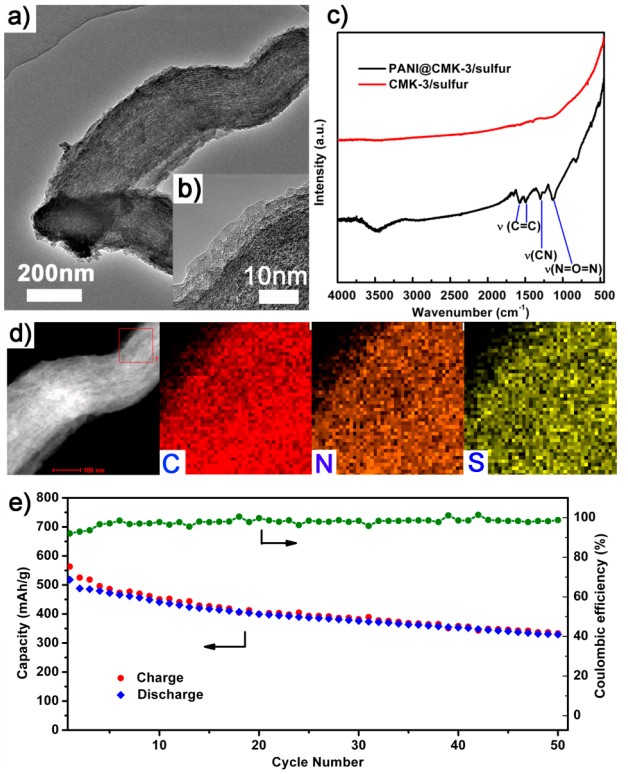

Figure 5. Instrumental analyses of PANI@CMK-3/sulfur composite: (a) TEM; (b) HRTEM; (c) FTIR spectra; (d) TEM and corresponding element mapping of C, N, and S in the red square area; (e) cycling performance and Coulombic efficiency at a current rate of 50 mA g^{-1}.

not changed after PANI coating. From the margin of the composite (Figure 5b), we can see that the average thickness of PANI is about 10 nm. Figure 5d shows the homogeneous distribution of the elements C, N, and S in the PANI@CMK-3/sulfur composite. The Fourier transform infrared (FTIR) spectra (Figure 5c) exhibit the characteristic peaks of PANI.[50−53] The broad peak located at 3400 cm^{-1} is due to the stretching vibration of N−H in an aromatic amine. The basic molecular of PANI with C═C stretching vibration bands of quinoid (Q) and benzenoid rings are located at 1580 and 1491 $cm^{-1.}$ The peak at 1301 cm^{-1} is due to the C−N stretching mode in an aromatic amine. The typical N═Q═N stretching band of PANI is observed at 1125 cm^{-1}. XRD patterns (Figure S6a, Supporting Information) shows that no peaks of sulfur were detected, while SEM images (Figure S6b, Supporting Information) show obvious changes on the surface of CMK-3. The final content of S in PANI@CMK-3/sulfur composite is 39.2 wt % according to the results of TG analysis (Figure S7, Supporting Information). Thus, it is credible that the coating of PANI was successfully well-proportioned on the surface of CMK-3/sulfur composite. The PANI@CMK-3/sulfur composite was assembled into K-S batteries as in the method above. The initial discharge capacity is 523.5 mAh g^{-1}, and the capacity was 329.3 mAh g^{-1} after 50 cycles (Figure 5e). In addition, the Coulombic efficiencies were all above 95% except for the first three cycles. Due to the overactive properties of metal K, the dissolved polysulfides were more easily reduced on the anode in comparison to Li-S batteries, which cause the cycling performance to be not quite satisfactory. However, in comparison with an uncoated cathode, the cycle performance was markedly improved, as the capacity retention increased from 39.4% to 62.9%.

In order to find the reason that PANI coating is an effective strategy to protect the structure of the cathode and impede the solvation of polysulfides, the testing cells were taken apart to observe the change in morphology before and after cycling. The surface without PANI coating collapsed after 50 cycles (Figure 6a,b). At the end of the charge, high-chain polysulfides were

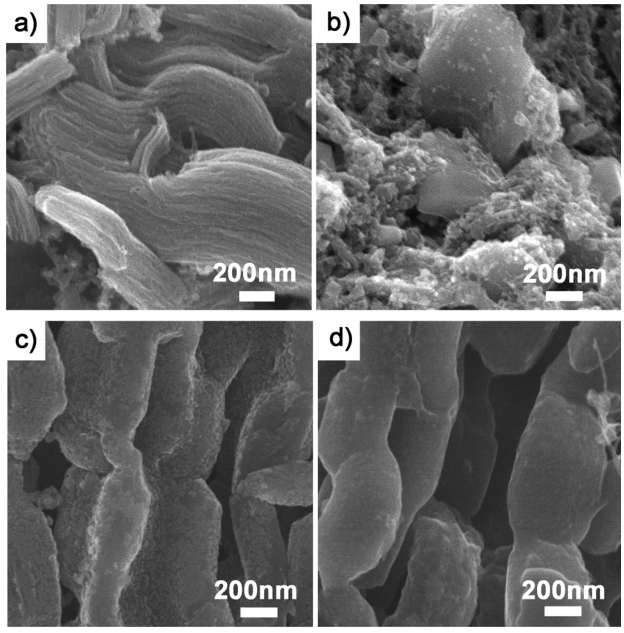

Figure 6. SEM images of (a) the initial CMK-3/sulfur cathode, (b) the cathode in (a) after 50 cycles, (c) the initial PANI@CMK-3/sulfur cathode, and (d) the cathode in (c) after 50 cycles.

partially dissolved into the electrolyte and shuttled into the metal side. Due to the overactive properties of K, the high-chain polysulfides were easily reduced to low-chain polysulfides on the surface of the K anode. Therefore, the diaphragm turned brown and the K anode was covered with yellow precipitates (Figure S8c,f, Supporting Information). In comparison, sulfur was trapped on the surface of PANI, and the structure of the PANI-coated cathode was well preserved after 50 cycles (Figure 6c,d). The diaphragm and the K anode are also well protected (Figure S8b,e, Supporting Information). The solvation of polysulfides would also cause a mass loss of sulfur. In comparison with the CMK-3/sulfur cathode with the loss of 62% of sulfur, the PANI-coated cathode only showed the loss of 28% of sulfur after 50 cycles. From the evidence above, it was confirmed that PANI coating was helpful in protecting the whole structure of the cathode and impeded the solvation of polysulfides.

To further analyze the process of rechargeable K-S batteries, the discharge and charge products were characterized. After

dx.doi.org/10.1021/ic500919e | Inorg. Chem. 2014, 53, 9000−9005

discharge, the TEM image of the product (Figure 7a) shows that the pores are filled, while the HRTEM image (Figure 7b)

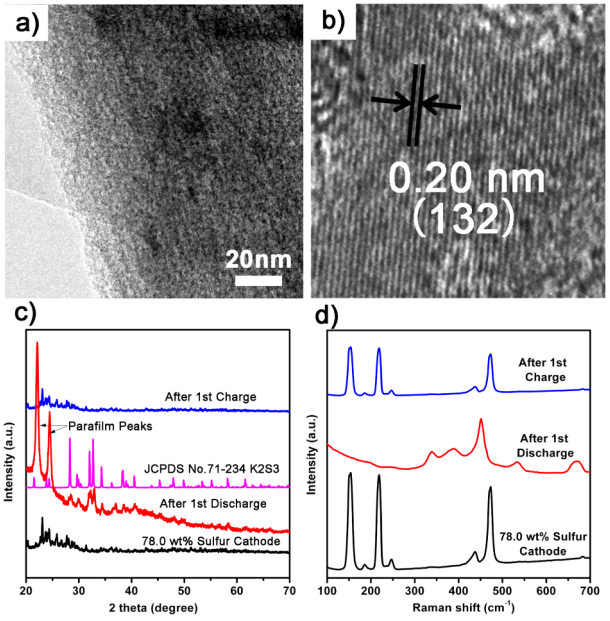

Figure 7. Characterization of CMK-3/sulfur cathode with 78.0 wt % S in K-S batteries: (a) TEM and (b) HRTEM after the first discharge; (c) XRD patterns with selected states in comparison with the standard JCPDS card of K_2S_3; (d) Raman spectra in selected processes.

displays the crystal face of K_2S_3. The corresponding element mapping (Figure S9, Supporting Information) shows a homogeneous distribution of C, S, and K. In the meantime, XRD patterns of the cathode after discharge (red line in Figure 7c) are quite in agreement with the standard card of K_2S_3 (other XRD spectra of K_2S_x are given in Figure S10, Supporting Information). The peaks of sulfur reappear after charge (blue line in Figure 7c). Furthermore, after discharge, the peaks of sulfur disappear and other new peaks appear in Raman spectra (red line in Figure 7d). The signals of sulfur reappear after charge (blue line in Figure 7d). In combination with the above analyses of TEM, XRD, and Raman, we know that sulfur reacts with K^+ (and electrons) to form K_2S_3 during the discharge, while K_2S_3 decomposes to sulfur and K^+ (and electrons) during charge. The overall reaction is the reversible reaction between 3S + 2K and K_2S_3. According to the electrochemical reaction, the degree of volumetric change between S and K_2S_3 can be calculated through the different densities of K_2S_3 (2.12 g cm $^{-3}$) and S (2.03 g cm^{-3}). S/K_2S_3 volumetric expansion/shrinkage during charge and discharge is about 73%.

It is noted that K_2S_3 was detected as the major product in K-S batteries, which is different in that the discharge product is Li_2S in Li-S batteries. The reason could be analogous to the case for Na−S batteries, where Na_2S_x ($x \geq 2$) is the final discharge product.[12] Solid sulfur usually shows low reactivity with metal potassium in liquid electrolyte, which leads to incomplete reduction to form polysulfides (K_2S_3) rather than K_2S. As Li_2S is considered as a promising cathode material which could lead to metal-free Li-S batteries,[54−56] K_2S_3 could also be used as a cathode material just like Li_2S. This could form a K ion battery without using metal potassium.

CONCLUSIONS

Potassium−sulfur batteries were assembled in the laboratory, and the charge−discharge mechanism was also illustrated. In comparison with Li-S batteries, K-S batteries have a similar charge−discharge process but with the different discharge product of K_2S_3. The reversible reaction of 3S + 2K to K_2S_3 has a role in this. In addition, a slightly higher discharge platform in comparison to that in room-temperature Na-S batteries was observed. Moreover, PANI coating was an effective method to protect the structure of the cathode with improved cycling performance. As a new battery system, rechargeable K-S batteries should enrich the family of batteries.

ASSOCIATED CONTENT

Supporting Information

Figures and a table giving TGA curves, TEM elemental mappings, SEM images, wide-angle XRD patterns, and BET, TEM, and corresponding element mapping. This material is available free of charge via the Internet at http://pubs.acs.org.

AUTHOR INFORMATION

Corresponding Author

*E-mail for J.C.: chenabc@nankai.edu.cn.

Notes

The authors declare no competing financial interest.

ACKNOWLEDGMENTS

This work was supported by the National Programs of 973 (2011CB935900), NSFC (21231005), and MOE (B12015, 113016A, and IRT13R30).

REFERENCES

(1) Manthiram, A.; Fu, Y. Z.; Su, Y. S. *Acc. Chem. Res.* **2013**, *46*, 1125−1134.
(2) Xin, S.; Gu, L.; Zhao, N. H.; Yin, Y. X.; Zhou, L. J.; Guo, Y. G.; Wan, L. J. *J. Am. Chem. Soc.* **2012**, *134*, 18510−18513.
(3) Yang, Y.; Zheng, G. Y.; Cui, Y. *Chem. Soc. Rev.* **2013**, *42*, 3018−3032.
(4) Cakan, R. D.; Morcrette, M.; Nouar, F.; Davoisne, C.; Devic, T.; Gonbeau, D.; Dominko, R.; Serre, C.; Férey, G.; Tarascon, J. M. *J. Am. Chem. Soc.* **2011**, *133*, 16154−16160.
(5) Guo, J. C.; Yang, Z. C.; Yu, Y. C.; Abruña, H. D.; Archer, L. A. *J. Am. Chem. Soc.* **2013**, *135*, 763−767.
(6) Zhang, K.; Zhao, Q.; Tao, Z. L.; Chen, J. *Nano Res.* **2013**, *6*, 38−46.
(7) Wang, L.; Wang, D.; Zhang, F. X.; Jin, J. *Nano Lett.* **2013**, *13*, 4206−4211.
(8) Wang, L. J.; Zhang, T. R.; Yang, S. Q.; Cheng, F. Y.; Liang, J.; Chen, J. *J. Energy Chem.* **2013**, *22*, 72−77.
(9) Zhou, G. M.; Pei, S. F.; Li, L.; Wang, D. W.; Wang, S. G.; Huang, K.; Yin, L. C.; Li, F.; Chen, H. M. *Adv. Mater.* **2014**, *26*, 625−631.
(10) Hwang, T. H.; Jung, D. S.; Kim, J. S.; Kim, B. G.; Choi, J. W. *Nano Lett.* **2013**, *13*, 4532−4538.
(11) Lee, D. J.; Park, J. W.; Hasa, I.; Sun, Y. K..; Scrosati, B.; Hassoun, J. *J. Mater. Chem. A* **2013**, *1*, 5256−5261.
(12) Xin, S.; Yin, Y. X.; Guo, Y. G.; Wan, L. J. *Adv. Mater.* **2014**, *26*, 1261−1265.
(13) Zheng, S. Y.; Han, P.; Han, Z.; Li, P.; Zhang, H. J.; Yang, J. H. *Adv. Energy. Mater.* **2014**, DOI: 10.1002/aenm.201400226.
(14) Cheng, F. Y.; Liang, J.; Tao, Z. L.; Chen, J. *Adv. Mater.* **2011**, *23*, 1695−1715.
(15) Park, C. W.; Ahn, J. H.; Ryu, H. S.; Kim, K. W.; Ahn, H. J. *Electrochem. Solid-State Lett.* **2006**, *9*, A123−A125.
(16) Ryu, H.; Kim, T.; Kim, K.; Ahn, J. H.; Nam, T.; Wang, G. X.; Ahn, H. J. *J. Power Sources* **2011**, *196*, 5186−5190.

(17) Kim, H. S.; Arthur, T. S.; Allred, G. D.; Zajicek, J.; Newman, J. G.; Rodnyansky, A. E.; Oliver, A. G.; Boggess, W. C.; Muldoon, J. *Nat. Commun.* **2011**, *2*, 427.
(18) Yoo, H. D.; Shterenberg, I.; Gofer, Y.; Gershinsky, G.; Pour, N.; Aurbach, G. *Energy. Environ. Sci.* **2013**, *6*, 2265−2279.
(19) Ha, S. Y.; Lee, Y. W.; Woo, S. W.; Koo, B.; Kim, J. S.; Cho, J.; Lee, K. T.; Choi, N.-S. *ACS Appl. Mater. Interfaces* **2014**, *6*, 4063−4073.
(20) See, K. A.; Gerbec, J. A.; Jun, Y. A.; Wudl, F.; Stucky, G. D.; Seshadri, R. *Adv. Energy Mater.* **2013**, *3*, 1056−1061.
(21) Ren, X. D.; Wu, Y. Y. *J. Am. Chem. Soc.* **2013**, *135*, 2923−2926.
(22) Cheng, F. Y.; Chen, J. *Chem. Soc. Rev.* **2012**, *41*, 2172−2192.
(23) Wessells, C. D.; Peddada, S. V.; Huggins, R. A.; Cui, Y. *Nano Lett.* **2011**, *11*, 5421−5425.
(24) Hu, Y. X.; Han, X. P.; Cheng, F. Y.; Zhao, Q.; Hu, Z.; Chen, J. *Nanoscale* **2014**, *6*, 177−180.
(25) Cheng, F. Y.; Shen, J.; Peng, B.; Pan, Y. D.; Tao, Z. L.; Chen, J. *Nat. Chem.* **2011**, *3*, 79−84.
(26) Wei, W.; Pol, V. G.; Amine, K. *Adv. Mater.* **2013**, *25*, 1608−1615.
(27) Aso, K.; Sakuda, A.; Hayashi, A.; Tatsumisago, M. *ACS Appl. Mater. Interfaces* **2013**, *5*, 686−690.
(28) Ji, X. L.; Nazar, L. F. *J. Mater. Chem.* **2010**, *20*, 9821−9826.
(29) Wang, D. W.; Zeng, Q. C.; Zhou, G. M.; Yin, L. C.; Li, F..; Cheng, H. M.; Gentle, I. R.; Lu, G. Q. *J. Mater. Chem. A* **2013**, *1*, 9382−9394.
(30) Jayaprakash, N.; Shen, J.; Moganty, S. S.; Corona, A.; Archer, L. A. *Angew. Chem., Int. Ed.* **2011**, *50*, 5904−5908.
(31) Zhang, K.; Hu, Z.; Chen, J. *J. Energy Chem.* **2013**, *22*, 214−225.
(32) Lu, S. T.; Cheng, Y. W.; Wu, X. H.; Liu, J. *Nano Lett.* **2013**, *13*, 2485−2489.
(33) Guo, J. C.; Xu, Y. H.; Wang, C. S. *Nano Lett.* **2011**, *11*, 4288−4294.
(34) Gao, X. F.; Li, J. Y.; Guan, D. S.; Yuan, C. *ACS Appl. Mater. Interfaces.* **2014**, *6*, 4154−4159.
(35) Lee, J. T.; Zhao, Y. Y.; Thieme, S.; Kim, H.; Oschatz, M.; Borchardt, L.; Magasinski, A.; Cho, W.; Kaskel, S.; Yushin, G. *Adv. Mater.* **2013**, *25*, 4573−4579.
(36) Lacey, M. J.; Jeschull, F.; Edström, K.; Brandell, D. *Chem. Commun.* **2013**, *49*, 8531−8533.
(37) Jun, S.; Joo, S. H.; Ryoo, R.; Kruk, M.; Jaroniec, M.; Liu, Z.; Ohsuna, T.; Terasaki, O. *J. Am. Chem. Soc.* **2000**, *122*, 10712−10713.
(38) Li, H.; Duan, W.; Zhao, Q.; Cheng, F.; Liang, J.; Chen, J. *Inorg. Chem. Front.* **2014**, *1*, 193−199.
(39) Ji, X. L.; Lee, K. T.; Nazar, L. F. *Nat. Mater.* **2009**, *8*, 500−506.
(40) Zhang, K.; Li, J.; Li, Q.; Fang, J.; Zhang, Z. A.; Lai, Y. Q.; Tian, Y. J. *Appl. Surf. Sci.* **2013**, *285*, 900−906.
(41) Yin, L. C.; Wang, J. L.; Lin, F. J.; Yang, J.; Nuli, Y. N. *Energy Environ. Sci.* **2012**, *5*, 6966−6972.
(42) Xiao, L. F.; Cao, Y. Y.; Xiao, J.; Schwenzer, B.; Engelhard, M. H.; Saraf, L. V.; Nie, Z. M.; Exarhos, G. J.; Liu, J. *J. Mater. Chem. A* **2013**, *1*, 9517−9526.
(43) Cheng, F. Y.; Ma, H.; Li, Y. M.; Chen, J. *Inorg. Chem.* **2007**, *46*, 788−794.
(44) Zhang, X. L.; Cheng, F. Y.; Yang, J. G.; Chen, J. *Nano Lett.* **2013**, *13*, 2822−2855.
(45) Zhu, Z. Q.; Wang, S. W.; Du, J.; Jin, Q.; Zhang, T. R.; Cheng, F. Y.; Chen, J. *Nano Lett.* **2014**, *14*, 153−157.
(46) Qin, W.; Hu, B. G.; Bao, D.; Gao, P. *Int. J. Hydrogen Energy* **2014**, *39*, 9300−9306.
(47) Cheng, F. Y.; Zhao, J. Z.; Song, W. E.; Li, C. S.; Ma, H.; Chen, J.; Shen, P. W. *Inorg. Chem.* **2006**, *45*, 2038−2044.
(48) Wang, S. W.; Wang, L. J.; Zhang, K.; Zhu, Z. Q.; Tao, Z. L.; Chen, J. *Nano Lett.* **2013**, *13*, 4404−4409.
(49) Ma, H.; Zhang, S. Y.; Ji, W. Q.; Tao, Z. L.; Chen, J. *J. Am. Chem. Soc.* **2008**, *130*, 5361−5367.
(50) Xia, X. H.; Chao, D. L.; Qi, X. Y.; Xiong, Q. Q.; Zhang, Y. Q.; Tu, J. P.; Zhang, H.; Fan, H. J. *Nano Lett.* **2013**, *13*, 4562−4568.
(51) Zhou, W. D.; Yu, Y. C.; Chen, H.; DiSalvo, F. J.; Abruña, H. D. *J. Am. Chem. Soc.* **2013**, *135*, 16736−16743.
(52) Zhang, F.; Cao, H. Q.; Yue, D. M.; Zhang, J. X.; Qu, M. Z. *Inorg. Chem.* **2012**, *51*, 9544−9451.
(53) Nan, C. Y.; Lin, Z.; Liao, H.-G.; Song, M.-K.; Li, Y. D.; Cairns, E. J. *J. Am. Chem. Soc.* **2014**, *136*, 4659−4663.
(54) Cai, K. P.; Song, M. K.; Cairns, E. J.; Zhang, Y. G. *Nano Lett.* **2012**, *12*, 6474−6479.
(55) Lin, Z.; Liu, Z. C.; Dudney, N. J.; Liang, C. D. *ACS Nano* **2013**, *7*, 2829−2833.
(56) Yang, Y.; Zheng, G. Y.; Misra, S.; Nelson, J.; Toney, M. F.; Cui, Y. *J. Am. Chem. Soc.* **2012**, *134*, 15387−15394.